State-Space Detection of the Impulse Response Gain and Delay From Intra-Partum Cardiotocography

Philip A Warrick[1] and Emily F Hamilton[1,2]

[1] PeriGen, Inc, Montreal, Canada
[2] Department of Obstetrics and Gynecology, McGill University, Montreal, Canada

Abstract

Objective: We model the signals acquired from intra-partum cardiotocography (CTG), uterine pressure (UP) and fetal heart rate (FHR), as an input-output system to estimate its dynamics in terms of an impulse response function (IRF). We aim to demonstrate discrimination of the IRF gain between normal (N) and metabolic acidotic (MA) fetuses with the state-space subspace approach, which incorporates noise-suppression and permits the use of non-contiguous data. This is important because CTG data is very noisy and missing data are common. Methods: Recordings of 449 N, 419 MA and 85 severely pathological (P) fetuses were detrended and analyzed with 20-min processing epochs. Results: 3/6 epochs in the last 60 minutes of recording before delivery showed statistically significant differences in the class distributions of N and MA fetuses the model gain parameter.

1. Introduction

Labour and delivery is routinely monitored electronically with sensors that measure maternal uterine pressure (UP) and fetal heart rate (FHR), a procedure referred to as cardiotocography (CTG). Temporary decreases in FHR are known as decelerations and reflect events such as compression of the umbilical cord by uterine contractions, malfunction of the fetal heart muscle, or premature separation of the placenta. Generally, larger insults are indicated by recurring episodes of deep, long decelerations whose onsets occur late with respect to the uterine contractions. We extract information from UP-FHR by treating the pair as an input-output system using system identification to estimate system dynamics in terms of an impulse response function (IRF).

A significant challenge to such modelling is that CTG often contains intervals of missing data on the UP or FHR signals. Signals with non-contiguous intervals were ignored in [1, 2] using non-parametric linear regression, which is inapplicable to such data. In [3] we applied state-space techniques to extract more information from data with non-contiguous intervals using recordings from normal (N) and pathological (P) outcome classes. In this study we extended this technique and applied it to metabolic acidotic (MA) fetuses. These cases are important because they have experienced hypoxia to the extent of metabolic acidosis, yet have not sustained neurological injury. Detecting these cases before injury occurs could prevent pathological outcomes.

Increasing the number and amount of recordings amenable to analysis with a discriminating technique has the potential to warn clinicians on more cases and earlier on when intervention could potentially avert the pathological outcome. Using a database of CTG recordings labelled with these three outcome classes, we compared the models over the final three hours of labour.

2. Data

We used CTGs from singleton, term pregnancies having no known congenital malformations, with at least 90 min of tracing just prior to delivery. 449 the cases were normal (N), 419 had developed MA (umbilical cord base deficit $\leq$ 12 mmol/L) and 85 severely pathological (P) fetuses. The data come from hospitals that did routine umbilical cord blood gas measurements shortly after birth.

3. Methods

3.1. Overall processing

We modelled UP-FHR system dynamics by linear system identification. A preprocessing step cleaned and segmented the UP and FHR into 20 min epochs of input and output data ($\mathbf{u}$ and $\mathbf{f}$). Next, using subspace system-identification methods, we estimated the IRF $\hat{\mathbf{h}}$ and determined the best values for the IRF delay d.

3.2. Preprocessing

The CTG data was recorded at 4 Hz in a clinical setting, so it was subject to specific types of noise. The loss of

 ISSN: 2325-887X DOI: 10.22489/CinC.2018.367

sensor contact can temporarily interrupt the UP or FHR signals, and interference from the (much lower) maternal heart rate can corrupt the FHR. These both appeared in the signal as a sharp drop to much lower amplitude followed by a sharp signal restoration.

3.3. Linear model

Let the input, UP, and output, FHR, at time sample k ($k = 1 \ldots N$) be denoted by $u(k)$ and $f(k)$, respectively. The linear response $f(k)$ of a discrete-time system to an arbitrary input signal $u(k)$ is given by the convolution sum:

$$f(k) \quad = \quad \sum_{i=d}^{d+M-1} (h_i \Delta t) u(k-i) = \mathbf{h} * \mathbf{u}(\mathbf{k}) \quad (1)$$

where Δt is the sampling period, and $\mathbf{h}$ is the IRF beginning at delay sample d, and of length M. $\mathbf{u}(\mathbf{k})$ is the length-M vector of input samples $[u_{k-d-M+1} \ \ldots \ u_{k-d-1} \ u_{k-d}]$ used to compute $f(k)$ at sample k. For causal (physically realizable) systems, $d \geq 0$, but under certain conditions, such as input measurement delay, d may be negative [4].

3.4. Subspace method

A previous study directly estimated $\mathbf{h}$ above using linear regression and the pseudo-inverse of the input autocorrelation matrix [1]. This approach assumed contiguous input and output data (i.e., with gaps no greater than $15s$ in length). However, we wanted to relax this requirement in order to permit processing more of the data, which often included temporary gaps of longer duration.

Subspace methods are well-suited to this problem because they permit such non-contiguous data to be included in the estimation. In addition, they are very applicable to noisy data, such as CTG, because of their general noise model and inherent use of singular value decomposition (SVD) within a non-iterative, regression-based estimation. As well, by incorporating an estimate of initial state, all epoch data are used in subspace model estimates; data need not be discarded due to initial filter-length effects. Finally, they require very few tuning parameters apart from a scaling factor s.

The *PO-MOESP* subspace method [5] is based on a state-space input-output model that incorporates process and measurement noise, written in innovation form as:

$$\begin{aligned} x(k+1) &= Ax(k) + Bu(k) + Ke(k) \\ f(k) &= Cx(k) + Du(k) + e(k) \end{aligned} \quad (2)$$

where $x(k)$ is the state, the innovation $e(k)$ is a white-noise sequence and K is the Kalman gain. Whereas direct use of Kalman filter methods require matrices A, B, C and D to be specified, these parameters and the initial state $x(0)$ are all estimated by subspace methods. As in [3], we used the LTI-Toolbox [6] implementation of *PO-MOESP* for our single-input, single-output (SISO) state-space model estimates.

This avoids direct estimation of $\mathbf{h}$ and the need for length-M contiguous data as in (1), but $\mathbf{h}$ is available indirectly as

$$h(k) = \begin{cases} 0 & k < 0 \\ D & k = 0 \\ CA^{k-1}B & k > 0 \end{cases} \quad (3)$$

We found that using no direct feedthrough term (i.e., constraining D=0) produced the most consistent models with the best fidelity on the output prediction, as measured by the minimum description length (MDL).

The order r (i.e., the state-vector dimensionality) of the state-space model was selected by inspecting the most significant eigenvalues of the system matrix A. By experimentation, we found that regardless of the value of the maximum order s we provided, a system order $r = 2$ generally produced models with the best fidelity. This finding was consistent with a previous study that fitted a second-order continuous low-pass system to the IRF [7].

By varying s over selected values 2^j, $j = 3, 4, \ldots 7$, we produced multi-resolutional models that adapted to the time constants of the system. In this study we restricted j to 6 to be able to compare all models at the same resolution.

3.5. Delay detection

As described in [1], input measurement delay associated with the UP sensor may result in a negative IRF delay. In contrast, the physiological response is expected to have a positive delay. The combination of these two delays can produce an FHR response that occurs before (negative d) or after (positive d) the measured UP contraction onset. Therefore, we developed an algorithm to determine the best d for each epoch. We set the bounds on d to -20 to 80 s and ranked candidates according to their minimum description length (MDL).

4. Results

Table 1 shows the number of epochs processed and the number of valid epochs (i.e., epochs which produced successful models) for each class. Roughly half of the epochs were valid, with proportions of 50.4%, 49.5% and 47.8% for N, MA and P classes, respectively. These proportions were not different with statistical significance, as determined by the chi-square proportion test.

Fig. 1 shows the time progression of the model gain G for each class, showing the standard error about the mean.

Class	*nEpochs*	*nEpochs valid*	*%*
N	5116	608	50.4
MA	5667	2754	49.5
P	1235	2511	47.8

Table 1. Number of processed/valid epochs and percentage by class

The P cases were different from the N cases with statistical significance in 7 of the last 8 epochs (i.e., the last 75 min). The MA cases were different from the N cases in 3 of the last 6 epochs (i.e., the last 60,min). To better show the long tails of the per-epoch distributions, Fig. 2 shows the same time progression as a box and whisker plot. The model delay parameter d did not display significantly different results, mainly due to the fact that UP and FHR periodicity occasionally causes models with short delays to be chosen by the optimality criterion instead of long ones (and vice versa), causing noise in the delay estimates.

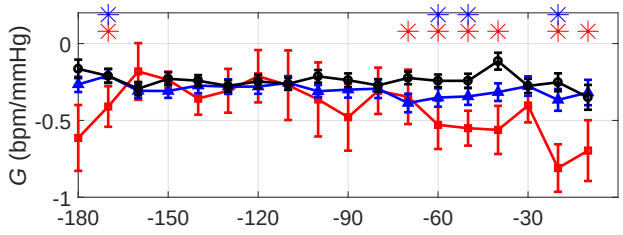

Figure 1. Time progression (mean±standard error) of model gain G for each class (N in black, MA in blue and P in red) in the last 180 min of labour and delivery. For each epoch, asterisks indicate statistically significant differences ($p < 0.05$, Kolmogorov-Smirnov test) between MA-N (blue) and P-N (red) class distributions, respectively.

5. Conclusions

We have shown that in addition to the statistically significant differences between P and N classes, which have been demonstrated in previous work [3], there are differences in the MA-N distributions. In addition, these differences appear 60 min before birth, allowing sufficient time to intervene with a Cesarian section. In future work, we will further examine whether the delay parameter d might be discriminating between MA and N cases.

6. Disclosure

This research was funded by PeriGen Inc.

References

[1] Warrick PA, Hamilton EF, Precup D, Kearney RE. Identification of the dynamic relationship between intra-partum uterine pressure and fetal heart rate for normal and hypoxic fetuses. IEEE Transactions on Biomedical Engineering June 2009;56(6):1587–1597.

[2] Warrick PA, Hamilton EF, Precup D, Kearney R. Classification of normal and hypoxic fetuses from systems modeling of intrapartum cardiotocography. IEEE Transactions on Biomedical Engineering 2010;57(4):771–779. ISSN 0018-9294.

[3] Warrick PA, Hamilton EF. Subspace detection of the impulse response function from intra-partum cardiotocography. In The 2011 IEEE Engineering in Medicine and Biology 33th Annual Conference. 2011; 5678–5681.

[4] Hunter IW, Kearney RE. Two-sided linear filter identification. Med Biol Eng Comput 1983;21:203–209.

[5] Verhaegen M, Verdult V. Filtering and system identification: a least squares approach. Cambridge, UK.: CUP, 2007.

[6] Verhaegen M, Verdult V, Bergboer N. The LTI-System Identification Toolbox, 2007. URL `http://www.dcsc.tudelft.nl/~jwvanwingerden`.

[7] Warrick PA, Kearney RE, Precup D, Hamilton EF. Low-order parametric system identification for intrapartum uterine pressure-fetal heart rate interaction. In The 2007 IEEE Engineering in Medicine and Biology 29th Annual Conference. 2007; 5043–5046.

Address for correspondence:

Philip A. Warrick
PeriGen Inc. (Canada)
245 Victoria Avenue, suite 600
Montreal, Quebec H3Z 3M6 Canada
philip.warrick@perigen.com

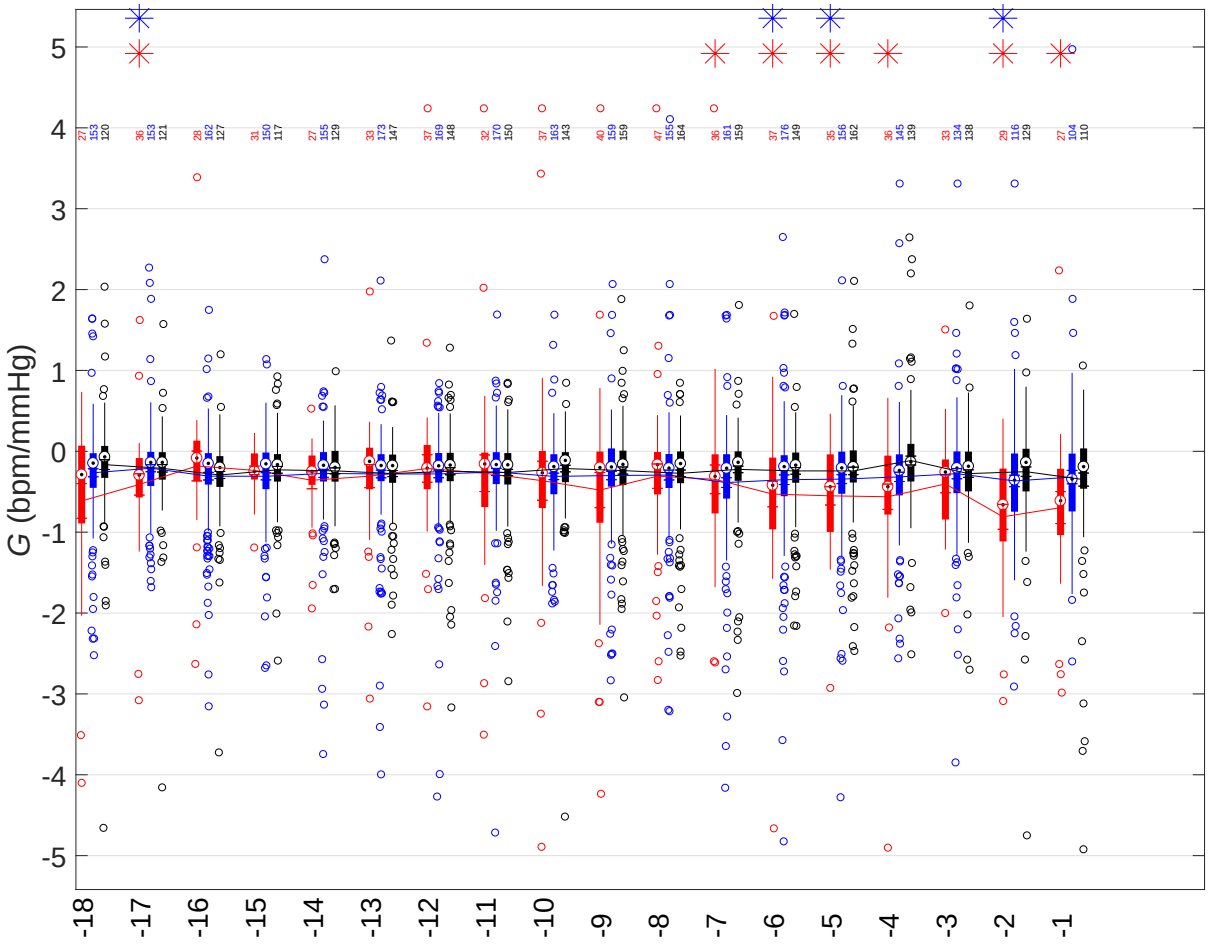

Figure 2. Time progression (box-whisker plot) of model gain G over time for each class, corresponding to Fig. 1. Boxes show interquartile range and whiskers include data within 150% of the interquartile width. The number of valid models at each epoch are also shown for each class. The x-axis show the epochs before delivery correspoding to the 10 min increments of Fig. 1